Magnetization transport in spin ladders and next-nearest-neighbor chains

Marko Žnidarič
Department of Physics, Faculty of Mathematics and Physics, University of Ljubljana, Ljubljana, Slovenia
(Dated: April 9, 2013)

We study magnetization transport at high temperatures in several spin ladder systems as well as in next-nearest-neighbor coupled spin chains. In the integrable ladder considered we analytically show that the transport is ballistic in sectors with nonzero average magnetization, while numerical simulations of a nonequilibrium stationary setting indicate an anomalous transport in the zero magnetization (half-filling) sector. For other systems, isotropic Heisenberg ladder and spin chains, showing eigenlevel repulsion typical of quantum chaotic systems, numerical simulations indicate diffusive transport.

I. INTRODUCTION

Understanding transport in quantum and classical systems from first principles has a long history. Perhaps the simplest question one can ask is what is the nature of transport in a given system, for instance, is it ballistic, in which case localized disturbances spread with time to a region whose size grows linearly with time, or, is it diffusive, in which case a region will grow as a square root of time. While the situation is clear in systems of non-interacting particles – in the absence of external scattering effects non-interacting systems are ballistic – for interacting systems (also called strongly correlated) such question proves to be very difficult to answer, even in the simplest conceivable models.

A paradigmatic example is, for instance, a one-dimensional Heisenberg model[1,2]. Although being originally devised as a toy model explaining high temperature of a ferromagnetic transition in metals, nowadays its anisotropic XXZ version serves as one of the simplest strongly interacting quantum systems. Despite being solvable by the Bethe ansatz[3] its nonequilibrium physics, in particular magnetization transport, is being debated for many years. The main obstacle one has to face trying to assess transport is a lack of efficient out-of-equilibrium tools, while on the other hand evaluating linear-response formalism using the Bethe-ansatz solution seems to be too difficult, except in the simplest case of zero temperature[4]. One exception are integrable systems for which the so-called Mazur's inequality[5,6] can be used to bound a current-current correlation function. Mazur's inequality states that if any of an infinite number of constants of motion that an integrable system possesses has a nonzero overlap with the current, the correlation function will not decay, thereby proving ballistic nature of transport. In the Heisenberg model this is for instance the case with energy transport[6,7] or magnetization transport away from zero-magnetization sector[6]. In the zero-magnetization (half-filling) sector though all known local constants of motion have, due to the spin-flip symmetry, zero overlap with the magnetization current[6] and no conclusion can be reached based on the Mazurs's inequality. Recently, a new quasi-local constant of motion has been found enabling one to prove ballistic transport in the gapless phase $|\Delta| < 1$[8,9]. For $|\Delta| \geq 1$ no rigorous results are known and one has to resort to numerical calculations making situation less clear, often even controversial. For $\Delta > 1$ and high temperatures magnetization transport seems to be diffusive[10–18], although more involved picture sometimes emerges[19,20]. Also at temperatures below the ground state gap theoretical arguments suggests diffusion[21]. Experimentally the most important, but at the same time also the most difficult for numerical studies, is the isotropic point. At isotropic point $\Delta = 1$ some numerical investigations suggest an anomalous transport[16,22,23], see also Ref. 24 for indications of an anomalous behavior at the isotropic point, while other[10,18,25–30] indicate ballistic transport or are inconclusive.

As the above example of an integrable 1d XXZ spin chain shows, transport behavior can be rather complex. At first sight appealing conjecture that, due to constants of motion, integrable systems display ballistic transport seems to be incorrect. Namely, as mentioned, an easy-axis XXZ Heisenberg chain shows strong evidence for diffusion. That solvability does not necessarily imply ballistic transport is indicated also by the existence of a solvable diffusive, albeit dissipative, 1d model[31]. Non-integrable, in general quantum chaotic[32] systems, are on the other hand expected to display diffusion. However, as recently demonstrated[33], there are exceptions to this rule. It has been rigorously shown that in a special class of an XX-type spin ladders (that class, for instance, includes the Hubbard chain) ballistic subspaces exist. Though probably exceptional, these counterexamples show that there are no general rules connecting, e.g., integrability or chaoticity, with the transport behavior. In light of this it is important to gather information on a transport type in different chaotic and integrable systems.

In the present work we shall study magnetization transport at high temperature in a number of spin ladder systems, including integrable and non-integrable ones. Transport, of either magnetization or heat, has been studied before[10,13,21,33–37] for some of the systems we consider, for other the presented results are new. Note that next-nearest-neighbor coupling terms, frequently used to break integrability in spin chains, in fact result in ladder systems. Therefore, some of the ladder systems

studied can also be considered as spin chains with next-nearest-neighbor (n.n.n.) coupling. We should also mention that spinfull particle chain models like, e.g., the 1d Hubbard model[4,11,19,21,38–45], can be, via Jordan-Wigner transformation, rewritten as spin ladder models. Spin ladder systems are not just of theoretical interest but are realized in a number of compounds, for a review see Refs. 46 and 47.

Apart from one integrable ladder, we shall exclusively focus on systems with strong chaos and at transport properties at high temperatures and half-filling. We shall demonstrate that the magnetization transport is diffusive in such systems. In the integrable ladder we on the other hand find anomalous transport at half-filling and analytically prove ballistic transport in sectors with non-zero magnetization.

II. METHODS

There are different ways to numerically assess quantum transport. One is via linear response theory by evaluating equilibrium time-dependent current autocorrelation function. In numerical calculations one is always limited to finite-size systems causing two effects: for finite L and time t the correlation function $C(t)$ might not yet converge to its thermodynamic limit value and, going with $t \to \infty$ the correlation function will not decay to zero, even in a diffusive system, but will rather have a finite-size fluctuations. Therefore, due to these finite-L and finite-t effects great care is needed to correctly evaluate the limits $\lim_{t\to\infty}\lim_{L\to\infty}$. Another way of studying transport is to directly simulate nonequilibrium states. There are two possibilities, one can study transient dynamics of initial nonequilibrium states like, e.g., spreading of localized packets and calculating how fast their width increases with time, or, one can go to a stationary setting in which a constant driving is applied to the system. The latter approach has the advantage that there are no finite-time effects, only finite-size, as one by definition studies a nonequilibrium stationary state reached after an infinite time. In present study we shall use a nonequilibrium stationary setting.

A. Lindblad master equation

Nonequilibrium situation will be induced by a boundary coupling to magnetization reservoirs. These can, with certain probabilities, flip the boundary spin either up or down. If these probabilities are different at two ladder ends the driving will cause a nonequilibrium state. Spin flips at the boundary are described in an effective way with the so-called Lindblad operators L_k, while the density matrix describing the ladder evolves according to the Lindblad master equation,

$$\mathrm{d}\rho(t)/\mathrm{d}t = \mathrm{i}[\rho(t), H] + \mathcal{L}^{\mathrm{dis}}(\rho(t)) = \mathcal{L}(\rho(t)), \qquad (1)$$

$$\mathcal{L}^{\mathrm{dis}}(\rho(t)) = \sum_k [L_k\rho(t), L_k^\dagger] + [L_k, \rho(t)L_k^\dagger].$$

Provided the dissipative part $\mathcal{L}^{\mathrm{dis}}$ is nonzero one will typically have a single stationary state ρ_∞, being the solution of $\mathcal{L}(\rho_\infty) = 0$, to which an arbitrary initial state $\rho(0)$ converges after long time, $\rho_\infty = \lim_{t\to\infty}\rho(t)$. In a nonequilibrium setting such a state ρ_∞ is called a nonequilibrium steady state (NESS).

Before specifying in detail Lindblad operators used, let us comment on the applicability of the Lindblad equation within the context of quantum transport. Lindblad equation can be derived from microscopic equations of motion of the system plus reservoirs under certain, from the condensed-matter perspective, rather restrictive conditions of a weak coupling and a fast decaying environmental correlations[48]. While these conditions are usually well satisfied in, e.g., quantum optical systems, where the environment is fast, this is not so in condensed matter. Environmental degrees there (electrons in the leads, phonons,...) are not necessarily fast compared to the timescale of the system of interest. As a consequence, evolution equation for the system will not be local in time, like the Lindblad equation (2), but will in general be non-local with a nontrivial integral kernel accounting for memory effects. While memory-effects can play a role in a transient finite-time behavior they are not expected to be important in the long time limit of nonequilibrium stationary states considered here. In certain situations one can even show exactly that memory effects, i.e., non-Markovian effects, play no role for NESS[49].

Lindblad operators modeling the reservoirs will differ depending on whether we want to study ladders or next-nearest-neighbor chains (that can be viewed as ladders with a diagonal inter-rung coupling, see Fig. 5). For ladders both spins in the first and in the last rung are coupled to the reservoir. Lindblad operators that we use are

$$\begin{aligned} L_{1,2} &= \sqrt{\Gamma(1\mp\mu)}\,\sigma_1^\pm, \quad L_{3,4} = \sqrt{\Gamma(1\pm\mu)}\,\sigma_L^\pm, \\ L_{5,6} &= \sqrt{\Gamma(1\mp\mu)}\,\tau_1^\pm, \quad L_{7,8} = \sqrt{\Gamma(1\pm\mu)}\,\tau_L^\pm, \end{aligned} \qquad (2)$$

where σ_k^α and τ_k^α are Pauli matrices on the 1st and the 2nd ladder leg, respectively, and $\sigma^\pm = (\sigma^{\mathrm{x}} \pm \mathrm{i}\,\sigma^{\mathrm{y}})/2$, $\tau^\pm = (\tau^{\mathrm{x}} \pm \mathrm{i}\,\tau^{\mathrm{y}})/2$ (in Eq.(2) upper and lower signs in $\pm$ go together). L is the number of rungs. For n.n.n coupled chains only the left-most and the right-most spins are coupled to reservoirs. Lindblad operators are

$$L_{1,2} = \sqrt{\Gamma}\sqrt{1\mp\mu}\sigma_1^\pm, \quad L_{3,4} = \sqrt{\Gamma}\sqrt{1\pm\mu}\sigma_L^\pm. \qquad (3)$$

For chains L is the chain length. The coupling Γ in both cases plays no essential role and we fix it to $\Gamma = 1$. The most important parameter is the driving μ. For zero driving $\mu = 0$ the NESS is a trivial $\rho_\infty \sim \mathbb{1}$, i.e., a equilibrium state at infinite temperature. For small μ the stationary state is a true nonequilibrium state, though it still stays close to an identity density matrix meaning that we are studying nonequilibrium systems at an infinite (high) temperature. Driving is also symmetric with

respect to the left/right end and the NESS obtained has always zero expectation value of the total magnetization (i.e., we are at half-filling). Note that the choice of actual Lindblad operators is quite arbitrary. The choice used in the present work is perhaps the simplest and has been used in a number of our previous studies, see also, e.g. Ref. 50. Provided the boundary effects are small, which is the case at high temperature[51], and for non-ballistic systems, the bulk properties should be independent of the details of driving.

Ladder and chain systems that shall be considered all conserve the total magnetization in the z direction. The corresponding unitary symmetry is $U = \exp(-\mathrm{i}\alpha \sum_j \sigma_j^z)$, with $UHU^\dagger = H$. Because a dissipative Lindblad term $\mathcal{L}^{\rm dis}$ (2,3) is also invariant under such U, nonequilibrium steady states considered in the present work are all independent of an optional homogeneous magnetic field in the z direction added to H. That is, if ρ_∞ is the NESS for $\mathcal{L}$ with H, then the same ρ_∞ is the NESS also for $\mathcal{L}'$ with $H' = H + B\sum_j \sigma_j^z$. This is a general consequence of the symmetry of the master equation. To see this let us denote by V a general unitary symmetry, and by C the corresponding conserved quantity. Let V be an exact symmetry of the Liouvillian (2), that is $V\mathcal{L}(\rho)V^\dagger = \mathcal{L}(V\rho V^\dagger)$. First, one notes that a unique NESS is invariant under V, $V\rho_\infty V^\dagger = \rho_\infty$, see e.g., Ref. 55. This means that in the eigenbasis of a corresponding conserved quantity C the matrix ρ_∞ is block-diagonal, while the matrix C is diagonal with identical elements within each diagonal block. C and ρ_∞ therefore commute and, if ρ_∞ satisfies $\mathrm{i}[\rho_\infty, H] + \mathcal{L}^{\rm dis}(\rho_\infty) = 0$, it also satisfies $\mathrm{i}[\rho_\infty, H + C] + \mathcal{L}^{\rm dis}(\rho_\infty) = 0$, i.e., ρ_∞ is also the NESS state for $H' = H + C$.

B. Numerical method

Because we want to study system's properties in a stationary state we have to obtain ρ_∞. There are two possibilities: one can either solve the stationary equation $\mathcal{L}(\rho_\infty) = 0$, or, one can integrate the Lindblad equation (2), obtaining $\rho(t)$ and from it the NESS in the limit $t \to \infty$. We use the latter method by first writing $\rho(t)$ in a matrix product form with matrices A_k^s of fixed dimension M, describing a site k and an element s of a local operator basis. Ladders as well as n.n.n. chains are treated as a ladder system with an arbitrary coupling between two nearest-neighbor rungs. One rung is considered as a single site k, so that the dimension of the operator basis at one site is 4^2 (i.e., the number of different values of the index s in matrices A_k^s). The total number of complex parameters describing a state $\rho(t)$ of a ladder with L rungs is therefore $16LM^2$. Choosing large enough M any state $\rho(t)$ can be written in such a matrix product operator form. Time evolution is then evaluated using the time-dependent density renormalization group method[52] by writing a short-time propagator $e^{\mathcal{L}\,\Delta t}$ as a series of single and two-site transformations. The method we use is an adaptation[12] for dissipative systems in which the optimality of a matrix product decomposition is preserved by reorthogonalizations, for details see Ref. 53. Evaluating two-site transformations exactly would lead to an exponentially increasing (in time) matrix dimension M. Numerically this can not be handled and one truncates dimension after each transformation to a fixed size M. This truncation is the main source of errors in the numerical method. How large should M be depends on the amount of entanglement that a state $\rho(t)$ has in the operator space. For instance, the equilibrium state at an infinite temperature is a product state (a product of identities at each site) and can be represented by matrices of size $M = 1$. For small μ, where $\rho(t)$ is still close to $\mathbb{1}$, we therefore expect that one can do with a reasonably small M. This is a reason why simulations of NESS at high temperatures require the smallest M. In our simulations we used matrix sizes of up-to $M = 150$ and ladder lengths of $L \leq 100$, requiring several weeks of simulation time for a single run on a 10-core CPU computer.

C. Assessing transport

Once the NESS is obtained – after time t that typically scales as an inverse power of L – expectation values of any local operator can be evaluated. Our main focus is on the magnetization current and on the magnetization profile along the ladder/chain. Fixing driving μ, typically at[54] $\mu = 0.2$, we study how magnetization current j scales with the system length L. If the scaling is $j \sim 1/L$, the system is diffusive and obeys a phenomenological transport law

$$j = -D\nabla z, \tag{4}$$

where ∇z is a magnetization gradient and D is a size-independent transport coefficient (diffusion constant). Other extreme situation would be when j is independent of L, signaling ballistic transport. Transport that is intermediate between ballistic and diffusive is called anomalous and is signaled by a scaling $j \sim 1/L^\alpha$ with $0 < \alpha < 1$. The nature of transport can be also inferred from magnetization profile. For small magnetization a profile is linear for diffusive systems while it is non-linear in the case of an anomalous transport where D can be considered to be length-dependent[22].

All above statements about the scaling should be investigated in the thermodynamic limit $L \to \infty$. Even though we limit ourselves, besides one integrable case, to fully chaotic systems, where the convergence with L is expected to be the fastest, it turns out that in some cases sizes $L \sim 100$, though rather large for a quasi-exact simulation of a strongly interacting quantum system, still might not be large enough to reach thermodynamic limit. Going to significantly larges sizes is at present not possible due to rapidly increasing simulation times. Simulation time increases with L because the convergence time to ρ_∞ increases, but even more significantly, the required

matrix size M also increases because the observables, like the current, decrease with L and so a larger M is required to obtain the same relative accuracy in j.

D. Checking for quantum chaos

Despite exceptions[33], one in general expects that for non-integrable strongly interacting quantum system, in other words for systems displaying characteristic features of quantum chaos, transport is diffusive. In order to convince ourselves that the systems we study are indeed not being close to integrability, we have checked their chaoticity by calculating the spacing distribution of nearest energy levels. The so-called level spacing distribution $p(s)$ is a standard criterion of quantum chaos in Hamiltonian systems[32]. In chaotic systems there are no selection rules and the eigenenergies will "repel" each other, leading to a deficit of small spacings between two consecutive eigenenergies. In quantum chaotic systems with time-reversal symmetry the expected theoretical level spacing distribution is well described by the so-called Wigner's surmise for the orthogonal ensemble,

$$p(s) = s\frac{\pi}{2}\exp\left(-s^2\pi/4\right). \tag{5}$$

In integrable system there are selection rules due to constants of motion, resulting in an exponential form of $p(s) = \exp(-s)$. One should bear in mind that in order to see chaotic level statistics (5) explicit symmetries of a system have to be taken into account. Spacing has to be calculated within a single symmetry class. The symmetries of the systems studied are described in Appendix A.

III. RESULTS FOR LADDERS

There has been a number of works studying magnetization transport[10,13,21,33] as well as heat transport[34–37] in spin ladders. For studies of transport in 1d Hubbard model, that can be equivalently rewritten as a spin ladder, see Refs. 4, 11, 19, 21, 38–45. The prevailing conclusion is that in non-integrable ladders at high temperature transport is diffusive, being in-line with a general rule of expecting diffusion in non-integrable systems. Numerical studies have been mostly limited to systems with less than $L = 20$ rungs; in present work we shall study significantly larger systems. For a review on ladder systems, including references to an extensive experimental work, see Refs. 46 and 47.

We shall name different ladder systems according to the type of the coupling between nearest-neighbor sites. XX-type is a coupling of the form $\sigma_i^{\rm x}\sigma_{i+1}^{\rm x}+\sigma_i^{\rm y}\sigma_{i+1}^{\rm y}$, XXZ-type is a coupling of the form $\sigma_i^{\rm x}\sigma_{i+1}^{\rm x}+\sigma_i^{\rm y}\sigma_{i+1}^{\rm y}+\Delta\sigma_i^{\rm z}\sigma_{i+1}^{\rm z}$, while an isotropic Heisenberg coupling is equal to the XXZ coupling with the anisotropy $\Delta = 1$, i.e., an XXX coupling.

Ladder systems that shall be studied are depicted in Fig. 1a and Fig. 1b. The same methodology that we use has been used before to study the so-called XX ladder, Fig. 1c, with an XX-type coupling along the legs and an XXZ-type in the rungs. A special case of such an XX ladder is the 1d Hubbard model obtained if the coupling in rungs is $\sigma_i^{\rm z}\tau_i^{\rm z}$. As shown in Ref. 44 the 1d Hubbard model is diffusive under symmetric driving at infinite temperature. This diffusive transport is not changed in the presence of an additional XX-type coupling in rungs[33]. It is instructive to rewrite a tight-binding system of free fermions on a ladder in spin language. Namely, for a tight-binding model we know that is is ballistic because it is equivalent to a system of free fermions. Using Jordan-Wigner transformation it can be written as a ladder shown in Fig. 1d with a 4-site coupling interchangeably connecting neighbors in the upper/lower leg being of the form $(\sigma_k^{\rm x}\sigma_{k+1}^{\rm x}+\sigma_k^{\rm y}\sigma_{k+1}^{\rm y})\tau_k^{\rm z}\tau_{k+1}^{\rm z}$ (written here for the upper leg). We have numerically checked (data not shown) that such a ladder coupling indeed results in ballistic magnetization transport. Note that the $\tau_k^{\rm z}\tau_{k+1}^{\rm z}$ term in the above coupling is absolutely crucial for the ballistic transport to appear; without it one would have an ordinary XX-type ladder displaying diffusive transport[33].

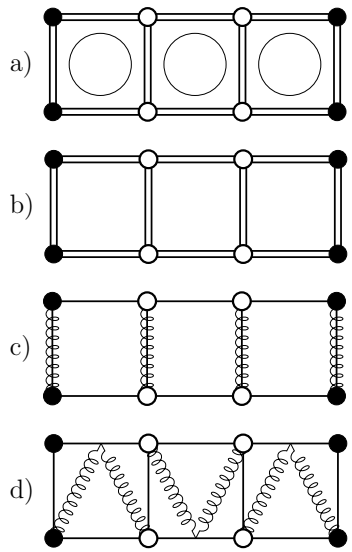

FIG. 1. Schematic representation of different spin ladders: a) integrable ladder, Eq. (7), b) isotropic Heisenberg ladder, Eq. (6), c) XX-ladder, d) free fermions on a ladder. Straight line denotes an XX-type coupling, spring a ZZ-type coupling, double line is an isotropic Heisenberg coupling while a straight line with two springs in d) is a coupling involving 4 sites (see text). Full points mark sites that are coupled to a reservoir, Eq. (2).

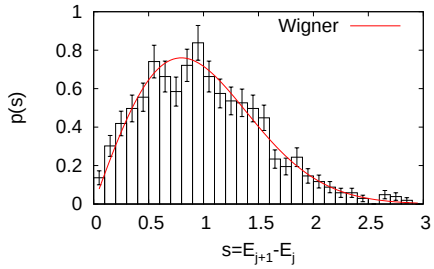

FIG. 2. Level spacing distribution for the isotropic Heisenberg ladder (6). $U = 1$, $L = 8$ and four symmetry sectors with $Z = 0$ and zero total spin size are used (1026 spacings in total), see Appendix A.

A. Isotropic Heisenberg ladder

Isotropic Heisenberg ladder is described by

$$H = \sum_{i=1}^{L-1} \boldsymbol{\sigma}_i \cdot \boldsymbol{\sigma}_{i+1} + \boldsymbol{\tau}_i \cdot \boldsymbol{\tau}_{i+1} + U \sum_{i=1}^{L} \boldsymbol{\sigma}_i \cdot \boldsymbol{\tau}_i. \quad (6)$$

Isotropic Heisenberg ladder, and in particular its version with different coupling strengths along rungs and legs ($U \neq 1$), is experimentally very much relevant[46,47]. The system (6) has a nonzero spin gap[56]. It is quantum chaotic as indicated by good agreement of level spacing distribution with the Wigner's surmise (5) demonstrated in Fig. 2.

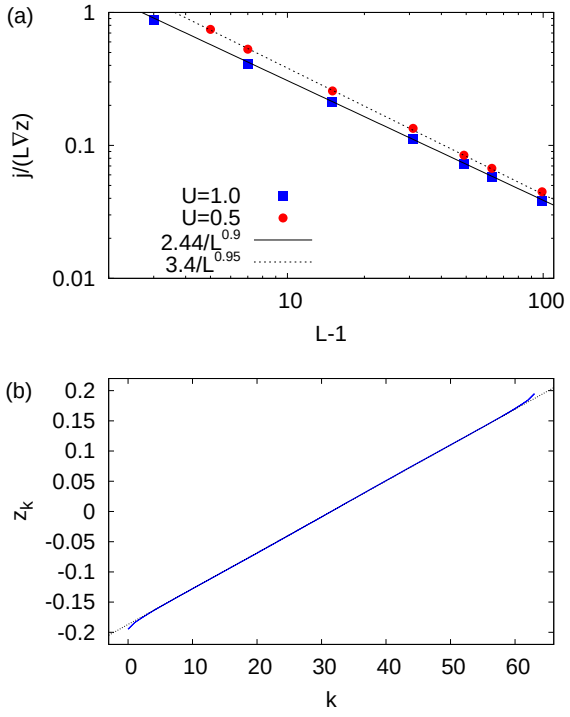

FIG. 3. a) Scaled magnetization current on L, b) magnetization profile in one of the chains ($U = 1, L = 64$). All for the isotropic Heisenberg ladder (6) and $\mu = 0.2$; in a) data for $U = 1.0$ and $U = 0.5$ is shown.

Regarding magnetization transport, in Ref. 13 it has been found that initial localized packets spread out diffusively. In our stationary nonequilibrium setting we use a symmetric driving of Eq. (2) so that in the NESS ρ_∞ magnetization flows only along both legs, and is equal in the two legs, while there is no current in the rungs. The current operator is defined via a continuity equation for local magnetization $\sigma^z_k + \tau^z_k$, resulting in $j^{\rm tot}_k = {\rm i}[\sigma^z_k + \tau^z_k, h_{k,k+1}]$, where $h_{k,k+1}$ is the local hamiltonian density. For the model in Eq.(6) we obtain $j^{\rm tot}_k = j^\sigma_k + j^\tau_k$, with the current operator in the upper leg $j^\sigma_k = 2(\sigma^{\rm x}_k\sigma^{\rm y}_{k+1} - \sigma^{\rm y}_k\sigma^{\rm x}_{k+1})$, and a similar expression for j^τ_k in the lower leg. Due to a symmetric driving of both legs (2) in NESS both currents are the same and, due to continuity, independent of the site k. We shall therefore simply study the current in one of the legs and denote $j = \langle j^\sigma_k \rangle = \langle j^\tau_k \rangle$, with averages being expectation values in the NESS ρ_∞. In Fig. 3 we show current and magnetization profile $z_k = {\rm tr}\,(\sigma^z_k \rho_\infty)$ in the NESS. At $\mu = 0.1$ the results would be almost indistinguishable from the presented ones for $\mu = 0.2$ in Fig. 3a. While magnetization profile is linear (with only very small deviations at few edge sites), suggesting diffusion, the scaling of the current shows small deviation from a diffusive $\sim 1/L$. At $U = 1.0$ the scaling is $j \sim 1/L^{0.9}$, while at $U = 0.5$ it is $j \sim 1/L^{0.95}$. Note that at $U = 0$ one would have two uncoupled isotropic Heisenberg chains for which an anomalous $j \sim 1/L^{0.5}$ scaling has been observed[16,22]. From the finite-size data presented it is difficult to make a definite conclusion whether magnetization transport in the Heisenberg ladder is diffusive or not in thermodynamic limit. Considering a rather linear magnetization profiles we deem it plausible that small deviations observed are due to finite-size effect and the transport would become diffusive in thermodynamic limit.

B. Integrable ladder

The Hamiltonian is

$$H = \sum_{j=1}^{L-1} (1 + \boldsymbol{\sigma}_j \cdot \boldsymbol{\sigma}_{j+1})(1 + \boldsymbol{\tau}_j \cdot \boldsymbol{\tau}_{j+1}) + 4U \sum_{j=1}^{L} \boldsymbol{\sigma}_j \cdot \boldsymbol{\tau}_j. \quad (7)$$

It is a Heisenberg ladder with an additional four-spin interaction[57]. At $U = 0$ the model is called a spin-orbital model[58] and can be obtained as a large-U limit of a two-orbital Hubbard model at quarter filling[59]. Spin-orbital model can be, up-to an irrelevant constant, written as $H_{\rm SU(4)} = H(U = 0) = \sum_j P_{j,j+1}$, where $P_{j,j+1}$ is a permutation operator on two rungs, $P_{j,j+1}|\alpha,\beta\rangle = |\beta,\alpha\rangle$, and $|\alpha\rangle, |\beta\rangle$ are two arbitrary rung states. Alternatively, it can be expressed in terms of generators $G^{\nu,\lambda} = |\nu\rangle\langle\lambda|$ of the SU(4) group, $H_{\rm SU(4)} \sim \sum_k \sum_{\nu,\lambda} G^{\nu,\lambda}_k G^{\lambda,\nu}_{k+1}$. Interaction is therefore SU(4) invariant and the spin-orbital

model can be considered to be a generalization of the isotropic Heisenberg chain (that has an SU(2) symmetry) and is sometimes called a SU(4) Heisenberg model. It is Bethe ansatz solvable in one dimension by the general method[60] for systems with permutation interaction. One-rung operators $C_1 = \sum_j \sigma_j^{\rm z} + \tau_j^{\rm z}$, $C_2 = \sum_j \sigma_j^{\rm z}\tau_j^{\rm z}$ and $C_3 = \sum_j \sigma_j^{\rm x}\tau_j^{\rm x} + \sigma_j^{\rm y}\tau_j^{\rm y} + \sigma_j^{\rm z}\tau_j^{\rm z}$ are conserved quantities for any U, while at $U = 0$ also all three components of $\sum_j \boldsymbol{\sigma}_j$ and $\sum_j \boldsymbol{\tau}_j$ are conserved. Nonzero rung interaction U (7), being equal to C_3, plays the role of a chemical potential, preserving integrability of the system[61] for any U. The model is gapless[61] for $U < 1$ and gapped for $U > 1$.

1. *Ballistic transport in nonzero-magnetization sectors*

Let us for a moment consider $H_{\rm SU(4)}$ obtained for $U = 0$. Because the Hamiltonian is a sum of nearest-neighbor transpositions one can easily construct invariant subspaces that will display ballistic transport. Taking the singlet $|S\rangle = (|01\rangle - |10\rangle)/\sqrt{2}$ and triplet states $|T\rangle = (|01\rangle + |10\rangle)/\sqrt{2}, |O\rangle = |00\rangle, |I\rangle = |11\rangle$ for a rung basis, and for instance the initial state of the ladder $|S\ldots SIIIS\ldots S\rangle$, we can see that $H_{\rm SU(4)}$ acting on such a state will cause the left-most and the right-most Is to spread ballistically to the left and right, respectively, causing two ballistic fronts. Although such construction is similar to the one in Ref. 33, two situations are fundamentally different. $H_{\rm SU(4)}$ is integrable, and, as we shall show, energy current is a constant of motion causing ballistic transport in sectors with nonzero magnetization, whereas the XX ladder discussed in Ref. 33 is quantum chaotic with a more complicated dynamics than just transpositions (for instance, there the energy current is not a constant of motion). To see why the model (7) is ballistic away from zero magnetization (half-filling) sector let us first define currents. The magnetization current operator is independent of U and is $j_k^{\rm tot} = j_k^{\sigma}(1+\boldsymbol{\tau}_k\cdot\boldsymbol{\tau}_{k+1}) + j_k^{\tau}(1+\boldsymbol{\sigma}_k\cdot\boldsymbol{\sigma}_{k+1})$, where $j_k^{\sigma,\tau}$ are the same chain currents as for the isotropic Heisenberg ladder. Local energy current, defined by $j_k^{\rm E} = {\rm i}[h_{k-1,k}, h_{k,k+1}]$, is a sum of an U-independent term and a term proportional to U, $j_k^{\rm E} = j_k^{\rm E}(U=0) + U\cdot j_k^{\rm E}(U\neq 0)$. $j_k^{\rm E}(U=0)$ is simply the energy current of the $H_{\rm SU(4)}$ model and is (written for $k = 2$)

$$j_2^{\rm E}(U=0) = [(\sigma_1^{\rm z} j_{23}^{\sigma} + \sigma_2^{\rm z} j_{31}^{\sigma} + \sigma_3^{\rm z} j_{12}^{\sigma}) \quad (8)$$
$$(\mathbb{1} + h_{12}^{\tau} + h_{13}^{\tau} + h_{23}^{\tau}) + (\sigma \leftrightarrow \tau)],$$

with $j_{jk}^{\sigma} = 2(\sigma_j^{\rm x}\sigma_k^{\rm y} - \sigma_j^{\rm y}\sigma_k^{\rm x})$ and $h_{jk}^{\tau} = \boldsymbol{\tau}_j\cdot\boldsymbol{\tau}_k$, and $(\sigma\leftrightarrow\tau)$ meaning all preceding terms with σ and τ matrices being interchanged. One can show that, taking periodic boundary conditions, the total energy current of the $H_{\rm SU(4)}$ model, $J_0^{\rm E} = \sum_k j_k^{\rm E}(U=0)$, is an exact constant of motion, $[J_0^{\rm E}, H] = 0$, regardless of U (note that $J^{\rm E} = \sum_k j_k^{\rm E}$ however, is not). Because $J_0^{\rm E}$ has in addition a nonzero overlap with the magnetization current it can be used to bound the spin Drude weight away from zero. Let us denote by $J^{\rm S} = \sum_k j_k^{\rm tot}$ the total magnetization current. Thermodynamic overlaps needed, e.g., $\langle J_0^{\rm E} J^{\rm S}\rangle$, are relatively simple to evaluate at infinite temperature but finite chemical potential, where the grand-canonical state is $\rho = \prod_k \rho_k$, with $\rho_k \sim \exp(-\phi\sigma_k^{\rm z})$ being an equilibrium state of one spin. Identifying $z = {\rm tr}\,(\rho_k\sigma_k^{\rm z})$ as the average equilibrium magnetization, or, equivalently, as the filling fraction $f = (z+1)/2$, all averages are polynomial functions of z. Denoting by $D_{\rm S}$ the magnetization Drude weight, Mazur's inequality[6] can be used to obtain

$$D_{\rm S} \geq \frac{\beta}{2}K, \qquad K = \frac{1}{L}\frac{\langle J_0^{\rm E} J^{\rm S}\rangle^2}{\langle J_0^{\rm E} J_0^{\rm E}\rangle}, \quad (9)$$
$$K = 2^9 \frac{z^2(1-z^2)(1+z^2)^2}{15 + 13z^2 + 10z^4 + 2z^6},$$

holding at high temperature. Observe that the bound is independent of U, simply because $J_0^{\rm E}$ and $J^{\rm S}$ are, even thou the Hamiltonian in Eq. (7) does depend on U. Away from maximal polarization, $z \neq \pm 1$, and nonzero magnetization, $z \neq 0$, the value of K is nonzero, proving nonzero spin Drude weight in the integrable spin ladder (7) at high temperature, and, as a consequence, ballistic magnetization transport. In present work we shall numerically study the case $z = 0$ ($f = 1/2$) where there remains a possibility to have non-ballistic transport.

2. *Numerical results for zero magnetization sector*

In numerical simulations we shall use the critical $U = 1$. Note however, that, due to the fact that the interaction term U is equal to the constant of motion C_3 of the closed system, magnetization transport for our symmetric driving is almost independent of the value of U. If the symmetry $V = \exp(-{\rm i}\alpha\sum_k \boldsymbol{\sigma}_k\cdot\boldsymbol{\tau}_k)$ corresponding to the conserved quantity $C_3 = \sum_k \boldsymbol{\sigma}_k\cdot\boldsymbol{\tau}_k$, would be an exact symmetry of the Liouvillian (2), $V\mathcal{L}(\rho)V^\dagger = \mathcal{L}(V\rho V^\dagger)$, then the NESS state ρ_∞ would be exactly independent of U. In our case the symmetry V preserves the unitary part, $VHV^\dagger = H$, but is not an exact symmetry of the dissipative part (2). Therefore, in an open system V is only an approximate symmetry; it is violated at boundaries. Still, we find[62] that the magnetization transport is almost independent of U. This also shows that the size of the ground state gap by itself does not play any role on transport at high temperatures.

In Fig. 4 we show the scaling[63] of magnetization current of one chain species $j \equiv \langle j_k^{\sigma}(1+\boldsymbol{\tau}_k\cdot\boldsymbol{\tau}_{k+1})\rangle$ with L and one instance of the magnetization profile. The current scales as $j \sim 1/L^{0.66}$, indicating anomalous transport. Correspondingly, magnetization profile along the ladder is not linear but rather displays larger gradients towards the ends. Similar profiles have been observed[16,22] in the isotropic Heisenberg model, also showing anomalous transport $j \sim 1/L^{\alpha}$ with $\alpha = 1/2$. Note that both, the isotropic Heisenberg model and the integrable ladder (7), are special due to their SU(2) and SU(4) sym-

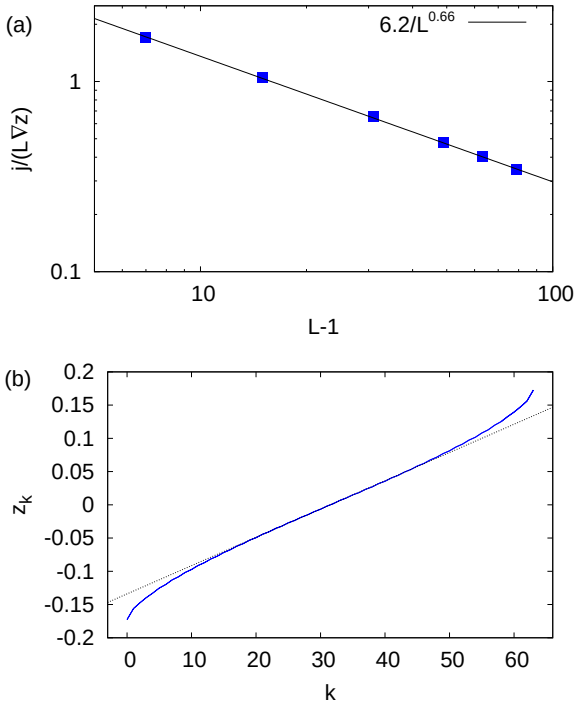

FIG. 4. a) Scaled magnetization current and b) magnetization profile in the upper leg ($L = 64$) for the integrable ladder system, Eq. (7). In b) the dotted line is the best-fitting gradient used in the scaling of current in frame a). $U = 1$, and driving $\mu = 0.2$.

metry, respectively. On a speculative note, considering that $\alpha = 1/2$ for the SU(2) model, and $\alpha = 2/3$ for the SU(4) one, general rule would be that the exponent of anomalous transport is $\alpha = N/(1 + N)$ for a model $H \sim \sum_k P_{k,k+1}$ with an SU(2N) invariance. This would suggest diffusive ($\alpha = 1$) transport in classical limit $N \to \infty$. For a recent study of transport in classical Heisenberg model see Ref.[64].

IV. NEXT-NEAREST-NEIGHBOR CHAINS

It is believed that integrability-breaking perturbations, provided they are large enough, will in general induce diffusive transport[10,12,20,25,28,65–67]. Some studies[26,68] observed indications of ballistic transport at low temperatures. In present work we reconsider the question of magnetization transport in spin chains with integrability-breaking next-nearest-neighbor coupling in the regime of strong integrability-breaking (quantum chaos). Different spin chains studied are shown in Fig. 5. Note that by numbering ladder sites in a zig-zag manner, the next-nearest-neighbor coupling of a chain is in the ladder formulation given by the coupling terms in both legs, while the nearest-neighbor coupling of the chain is the ladder coupling in rungs and the diagonal inter-rung coupling.

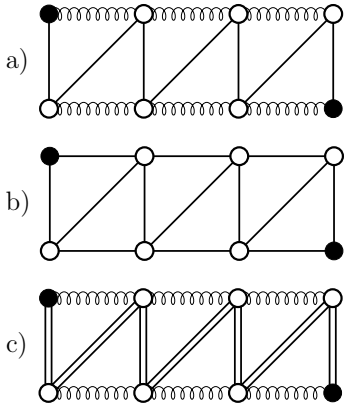

FIG. 5. Different spin chains with a next-nearest-neighbor coupling: a) XX chain with a ZZ n.n.n. coupling, b) XX chain with an XX n.n.n. coupling, c) isotropic Heisenberg chain with a ZZ n.n.n. coupling (a straight line is an XX-type coupling, a spring a ZZ-type coupling while a double line is an isotropic Heisenberg coupling). Full points mark the sites that are coupled to a reservoir (3).

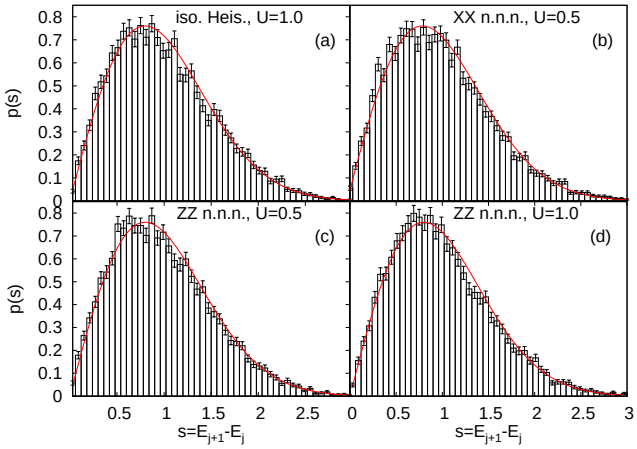

FIG. 6. Level spacing distribution for spin chains. a) Isotropic Heisenberg with a ZZ n.n.n. coupling, b) XX chain with a XX n.n.n. coupling, c) and d) XX chain with a ZZ n.n.n. coupling. All data is for $L = 8$ and a sector with $Z = 0$ (averaging over 4 subsectors; in total around 11000 levels for each system), see Appendix A. Full curve is the Wigner's surmize (5).

A. XX chain

First, we are going to study the XX chain with a ZZ next-nearest-neighbor coupling,

$$H = \sum_{i=1}^{L-1} (\sigma_i^{\rm x}\sigma_{i+1}^{\rm x} + \sigma_i^{\rm y}\sigma_{i+1}^{\rm y}) + U \sum_{i=1}^{L-2} \sigma_i^{\rm z}\sigma_{i+2}^{\rm z}. \qquad (10)$$

Magnetization current in the NESS is a standard $j = \langle 2(\sigma_k^{\rm x}\sigma_{k+1}^{\rm y} - \sigma_k^{\rm y}\sigma_{k+1}^{\rm x})\rangle$. Integrability breaking perturbation of strength $U = 0.5$ and $U = 1.0$ shall be used, for which the system is quantum chaotic. In Fig. 6 we can see nice agreement of level spacing distribution with the

Wigner's surmise.

We shall also study the XX chain with a XX type n.n.n. coupling,

$$H = \sum_{i=1}^{L-1} (\sigma_i^{\rm x}\sigma_{i+1}^{\rm x} + \sigma_i^{\rm y}\sigma_{i+1}^{\rm y}) + U \sum_{i=1}^{L-2} \sigma_i^{\rm x}\sigma_{i+2}^{\rm x} + \sigma_i^{\rm y}\sigma_{i+2}^{\rm y}. \quad (11)$$

At $U = 0.5$ studied the model is again quantum chaotic, see Fig. 6. Magnetization current operator gets in this case an additional next-nearest-neighbor term, and is

$$j_k = 2(\sigma_k^{\rm x}\sigma_{k+1}^{\rm y} - \sigma_k^{\rm y}\sigma_{k+1}^{\rm x}) + 2U(\sigma_k^{\rm x}\sigma_{k+2}^{\rm y} - \sigma_k^{\rm y}\sigma_{k+2}^{\rm x}). \quad (12)$$

As one can see in Fig. 7 magnetization transport is in all cases diffusive, indicated by the scaling $j \sim 1/L$, as well as by linear magnetization profiles.

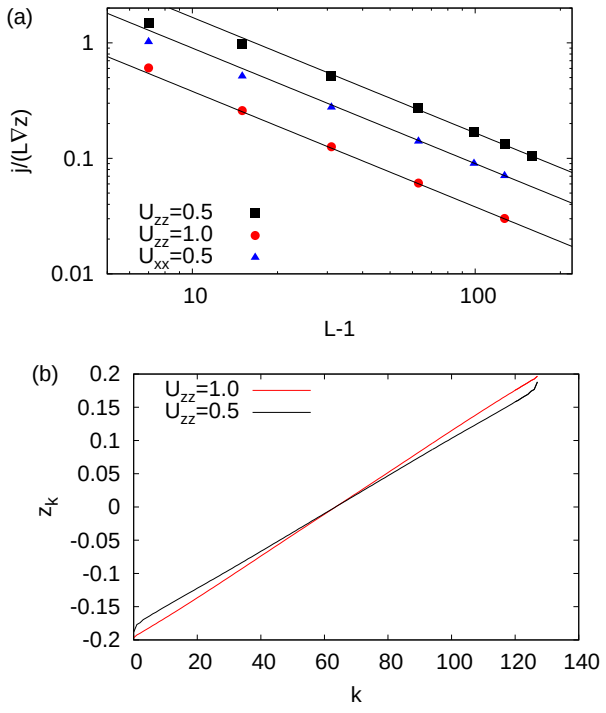

FIG. 7. a) Current scaling for the XX chain with a ZZ (squares and circles) or XX (triangles) type n.n.n. coupling. Scaling is in all cases diffusive. Straight lines are $16.6/L$, $9.0/L$ and $3.8/L$ (top to bottom). b) Magnetization profile is linear ($L = 128$). $\mu = 0.2$.

B. Isotropic Heisenberg chain

We also studied the Isotropic Heisenberg chain with a ZZ n.n.n. coupling,

$$H = \sum_{i=1}^{L-1} \boldsymbol{\sigma}_i \cdot \boldsymbol{\sigma}_{i+1} + U \sum_{i=1}^{L-2} \sigma_i^{\rm z}\sigma_{i+2}^{\rm z}, \quad (13)$$

and we shall use $U = 1.0$ for which the system is quantum chaotic, Fig. 6. Magnetization current is $j = \langle 2(\sigma_k^{\rm x}\sigma_{k+1}^{\rm y} - \sigma_k^{\rm y}\sigma_{k+1}^{\rm x})\rangle$. As shown in Fig. 8 the current scales as $j \sim 1/L^{1.1}$, while the profiles show slight deviations from a linear function close to chain ends. Note that, as is most often the case, if the current scales faster than $\sim 1/L$, i.e., if the system goes towards an insulating regime, a local gradient in profiles is smaller close to the system edge (Fig. 8), on the other hand, if the scaling is slower than $\sim 1/L$, i.e., if the system goes towards ballistic, the gradient is larger (e.g., Fig. 4). In the present case deviations are small and it is difficult to asses if it is just a finite size effect and the system becomes diffusive in thermodynamic limit.

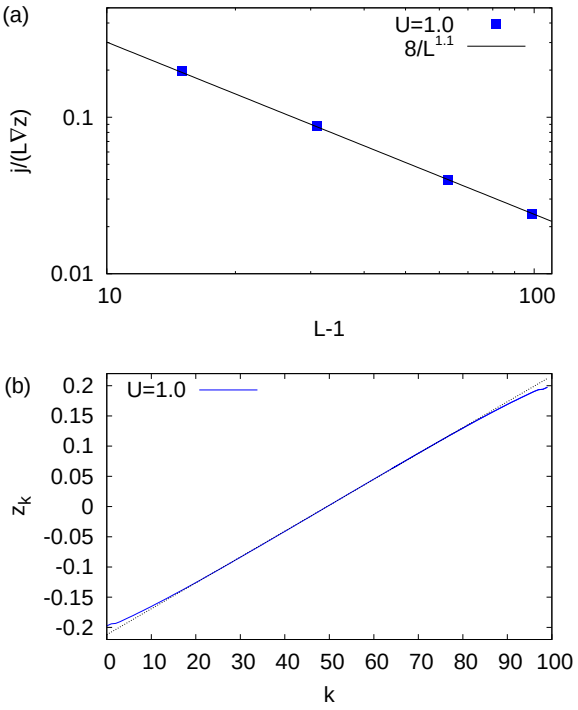

FIG. 8. The isotropic Heisenberg chain with a ZZ n.n.n. coupling of strength $U = 1.0$, $\mu = 0.2$. a) scaling of current with system size, b) magnetization profile for $L = 100$.

V. CONCLUSION

We have studied magnetization transport in a linear response regime at high temperature by numerically calculating nonequilibrium stationary states of Lindblad master equation. For the isotropic Heisenberg ladder, being quantum chaotic, we find close-to diffusive behavior, with the differences being possibly due to finite-size effects. In the XX spin chain with strong next-nearest-neighbor interaction transport is always found to be diffusive. The Isotropic Heisenberg chain with an integrability-breaking next-nearest-neighbor interaction is also very close to diffusive. We also found that the integrable ladder, which at $U = 0$ has a SU(4) symmetry, shows anomalous magnetization transport at half-filling, while away from half-

filling, using Mazur's inequality, we prove that the transport is ballistic.

ACKNOWLEDGMENTS

I acknowledge support by the program P1-0044 of Slovenian Research Agency.

Appendix A: Symmetries

We study magnetization transport, i.e., transport of the z-component of spin. All systems considered therefore conserve the total magnetization in the z-direction. For ladders this is the operator $Z = \sum_{j=1}^{L} \sigma_k^{\rm z} + \tau_k^{\rm z}$. The corresponding symmetry transformation is a rotation $U_{\rm z} = \prod_j \exp(-{\rm i}\alpha\sigma_j^{\rm z}) \exp(-{\rm i}\alpha\tau_j^{\rm z})$. Under U Pauli matrices transform as $U\sigma_k^{\rm z}U^\dagger = \sigma_k^{\rm z}$, $U\sigma_k^{\rm x}U^\dagger = \cos(2\alpha)\sigma_k^{\rm x} + \sin(2\alpha)\sigma_k^{\rm y}$, and $U\sigma_k^{\rm y}U^\dagger = -\sin(2\alpha)\sigma_k^{\rm x} + \cos(2\alpha)\sigma_k^{\rm y}$, and similarly for τ_k^α.

There are two geometrical symmetries of the underlying ladder lattice. One is a parity $P_{\rm x}$ in the x-direction, obtained by mapping of sites $k \to L+1-k$, while the other is a parity $P_{\rm y}$ in the y-direction, obtained by the swapping of the two legs, $\sigma_k^\alpha \leftrightarrow \tau_k^\alpha$.

In addition, there is a spin-flip symmetry given by the transformation $U = \prod_j \sigma_j^{\rm x}\tau_j^{\rm x}$, i.e., a rotation $\exp(-{\rm i}\pi\sigma^{\rm x}/2)$ around the x-axis. It changes the sign of $\sigma_k^{\rm y,z}$ while it preserves $\sigma_k^{\rm x}$. It commutes with the rotation $U_{\rm z}$ around z only in the sector with zero total magnetization $Z = 0$.

Symmetries of the isotropic Heisenberg ladder described by H in Eq. (6) are both parities $P_{\rm x}$ and $P_{\rm y}$, spin-flip and total magnetization Z. In addition, square of the total spin $(\sum_j \boldsymbol{\sigma}_j + \boldsymbol{\tau}_j)^2$ is also a constant of motion.

For chains with a n.n.n. coupling, Eqs. (10,11,13), the symmetries are spin-flip, total magnetization Z and a product of parities $P_{\rm x}P_{\rm y}$.

[1] W. Heisenberg, Z. Phys. **49**, 619 (1928).
[2] P. A. M. Dirac, Proc. R. Soc. Lond. A **123**, 714 (1929).
[3] H. Bethe, Z. Phys. A **71**, 205 (1931).
[4] B. S. Shastry and B. Sutherland, Phys. Rev. Lett. **65**, 243 (1990).
[5] P. Mazur, Physica **43**, 533 (1969).
[6] X. Zotos, F. Naef, and P. Prelovšek, Phys. Rev. B **55** 11029 (1997).
[7] M. P. Grabowski and P. Mathieu, Ann. Phys. (N.Y.) **243**, 299 (1995).
[8] T. Prosen, Phys. Rev. Lett. **106**, 217206 (2011).
[9] E. Ilievski and T. Prosen, Commun. Math. Phys. **318**, 809 (2013).
[10] F. Heidrich-Meisner, A. Honecker, D. C. Cabra, and W. Brenig, Phys. Rev. B **68**, 134436 (2003).
[11] P. Prelovšek, S. El Shawish, X. Zotos, and M. Long, Phys. Rev. B **70**, 205129 (2004).
[12] T. Prosen and M. Žnidarič, J. Stat. Mech. **(2009)**, P02035.
[13] S. Langer , F. Heidrich-Meisner, J. Gemmer, I. McCulloch, and U. Schollwöck, Phys. Rev. B **79**, 214409 (2009).
[14] R. Steinigeweg and J. Gemmer, Phys. Rev. B **80**, 184402 (2009).
[15] S. Jesenko and M. Žnidarič, Phys. Rev. B **84**, 174438 (2011).
[16] M. Žnidarič, Phys. Rev. Lett. **106**, 220601 (2011).
[17] S. Langer, M. Heyl, I. P. McCulloch, and F. Heidrich-Meisner, Phys. Rev. B **84**, 205115 (2011).
[18] C. Karrasch, J. H. Bardarson, and J. E. Moore, Phys. Rev. Lett. **108**, 227206 (2012).
[19] J. Sirker, R. G. Pereira, and I. Affleck, Phys. Rev. B **83**, 035115 (2011).
[20] R. Steinigeweg, J. Herbrych, P. Prelovšek, and M. Mierzejewski, Phys. Rev. B **85**, 214409 (2012).
[21] S. Sachdev and K. Damle, Phys. Rev. Lett. **78**, 943 (1997).
[22] M. Žnidarič, J. Stat. Mech. **(2011)**, P12008.
[23] J. Herbrych, R. Steinigeweg, and P. Prelovšek, Phys. Rev. B **86**, 115106 (2012).
[24] V. Popkov and M. Salerno, J. Stat. Mech. **(2013)** P02040.
[25] J. V. Alvarez and C. Gros, Phys. Rev. Lett. **88**, 077203 (2002).
[26] S. Fujimoto and N. Kawakami, Phys. Rev. Lett. **90**, 197202 (2003).
[27] J. Benz, T. Fukui, A. Klümper, and C. Scheeren, J. Phys. Soc. Jpn. Supp. **74**, 181 (2005).
[28] S. Mukerjee and B. S. Shastry, Phys. Rev. B **77**, 245131 (2008).
[29] S. Grossjohann and W. Brenig, Phys. Rev. B **81**, 012404 (2010).
[30] C. Karrasch, J. Hauschild, S. Langer, and F. Heidrich-Meisner, e-print arXiv:1301.6401.
[31] M. Žnidarič, J. Stat. Mech. (**2010**) L05002; M. Žnidarič, Phys. Rev. E **83**, 011108 (2011).
[32] F. Haake, *Quantum signatures of chaos*, 3rd ed. (Springer, Berlin, 2010).
[33] M. Žnidarič, Phys. Rev. Lett. **110**, 070602 (2013).
[34] J. V. Alvarez and C. Gros, Phys. Rev. Lett. **89**, 156603 (2002).
[35] E. Orignac, R. Chitra, and R. Citro, Phys. Rev. B **67**, 134426 (2003).
[36] X. Zotos, Phys. Rev. Lett. **92**, 067202 (2004).
[37] E. Boulat, P. Mehta, N. Andrei, E. Shimshoni, and A. Rosch, Phys. Rev. B **76**, 214411 (2007).
[38] C. A. Stafford, A. J. Millis, and B. S. Shastry, Phys. Rev. B **43**, 660 (1991).
[39] E. Jeckelmann, F. Gebhard, and F. H. L. Essler, Phys. Rev. Lett. **85**, 3910 (2000); R. M. Fye, M. J. Nartins, D. J. Scalapino, J. Wagner, and W. Hanke, Phys. Rev. B **44**, 6909 (1991).
[40] S. Fujimoto and N. Kawakami, J. Phys. A **31**, 465 (1998).
[41] S. Kirchner, H. G. Evertz, and W. Hanke, Phys. Rev. B **59**, 1825 (1999).

[42] N. M. R. Peres, R. G. Dias, P. D. Sacramento, and J. M. P. Carmelo, Phys. Rev. B **61**, 5169 (2000).
[43] S-J. Gu, N. M. Peres, and J. M. P. Carmelo, J. Phys.: Condens. Matter **19**, 506203 (2007).
[44] T. Prosen and M. Žnidarič, Phys. Rev. B **86**, 125118 (2012).
[45] J. M. P. Carmelo, S.-J. Gu, and P. D. Sacramento, e-print arXiv:1209.1276.
[46] M. T. Batchelor, X. W. Guan, N. Oelkers, and Z. Tsuboi, Adv. Phys. **56**, 465 (2007).
[47] E. Dagotto, Rep. Prog. Phys. **62**, 1525 (1999).
[48] H.-P. Breuer and F. Petruccione, *The Theory of Open Quantum Systems* (Oxford University Press, Oxford, 2002).
[49] S. Jesenko and M. Žnidarič, e-print arXiv:1303.2046.
[50] M. Michel, O. Hess, H. Wichterich, and J. Gemmer, Phys. Rev. B **77**, 104303 (2008).
[51] M. Žnidarič, T. Prosen, G. Benenti, G. Casati, and D. Rossini, Phys. Rev. E **81**, 051135 (2010).
[52] G. Vidal, Phys. Rev. Lett. **91**, 147902 (2003); F. Verstraete, J. J. Garcia-Ripoll, and J. I. Cirac, Phys. Rev. Lett. **93**, 207204 (2004); A. J. Daley, C. Kollath, U. Schollwöck, and G. Vidal, J. Stat. Mech. **(2004)**, P04005.
[53] M. Žnidarič, New J. Phys., **12**, 043001 (2010).
[54] $\mu = 0.2$ seems to be a good choice regarding numerical efficiency, while still being at the upper end of a linear response regime.
[55] V. Popkov and R. Livi, New J. Phys. **15**, 023030 (2013).
[56] T. Barnes, E. Dagotto, J. Riera, and E. S. Swanson, Phys. Rev. B **47**, 3196 (1993).
[57] A. A. Nersesyan and A. M. Tsvelik, Phys. Rev. Lett. **78**, 3939 (1997).
[58] Y. Q. Li, M. Ma, D. N. Shi, and F. C. Zhang, Phys. Rev. Lett. **81**, 3527 (1998).
[59] K. I. Kugel and D. I. Khomskii, Sov. Phys. JETP **37**, 725 (1973).
[60] B. Sutherland, Phys. Rev. B **12**, 3795 (1975).
[61] Y. Wang, Phys. Rev. B **60**, 9236 (1999).
[62] We have checked numerical simulations at $U = 0.3$ and $U = 0.0$ and they resulted in virtually the same $j(L)$ as for $U = 1.0$.
[63] Numerical simulations for the integrable ladder are somewhat more demanding than for other systems studied because the required matrix product operator dimension M is larger. Because of slower convergence with M we have used extrapolation in order to obtain the current j in the limit $M \to \infty$. The extrapolated value for $L = 80$ differed from the one at $M = 150$ by about 5 %.
[64] R. Steinigeweg, Europhys. Lett. **97**, 67001 (2012).
[65] X. Zotos and P. Prelovšek, Phys. Rev. B **53**, 983 (1996).
[66] A. Rosch and N. Andrei, Phys. Rev. Lett. **85**, 1092 (2000).
[67] Y. Huang, C. Karrasch, and J. E. Moore, e-print arXiv:1212.0012.
[68] D. Heidarian and S. Sorella, Phys. Rev. B **75**, 241104(R) (2007).